VISUALIZATION AND MEASUREMENTS OF BUBBLY TWO-PHASE FLOW STRUCTURE USING PARTICLE IMAGING VELOCIMETRY (PIV)

Hassan Abdulmouti, Associate Professor
Esam Jassim, Assistant Professor
Mechanical Engineering Dept. Prince Mohammad Bin Fahd University (PMU). Al Azezaya, Eastern Province, KSA

Abstract:

Gas injection through a bottom nozzle is very popular and has wide applications. Hence; many researchers have carried out extensive model experiments by focusing on flow field's structure using air bubbles. The bubble plume, which is a typical form of bubble flow, is known as one of the transport phenomena that have the capability to drive a large-scale convection due to the buoyancy of the bubbles. The technique of using a surface flow generated by the bubble plume is utilized as an effective way to control and collect surface floating substances in naval systems, lakes, seas, rivers, oceans especially the oil layer formed during large oil spill accidents. The surface flows generated by bubble plumes are considered to be key phenomena in various kinds of reactors, engineering processes and industrial processes handling a free surface. The motivation of this research is to broaden the understanding and demonstration of the following points: 1) The most important applications of bubbly flow and gas-liquid two-phase flow. 2) The differences of surface flow generation mechanisms among single-phase liquid jet, single phase buoyant plume, and bubble plume. 3) The relationship between the dominated parameters of bubbly flow that are demanded to describe the characteristics of the bubble generating surface flow. Such flow depends on the gas flow rate, the bubble size, void friction, bubble velocity and the internal two-phase flow structure of the bubble plume. Laboratory experiments have been carried out in order to investigate the multi-dimensional motion of water and bubbles. The data are obtained by applying image processing and Particle Imaging Velocimetry (PIV) measurements to two kinds of visualized images: The first is visualization of the whole field around the bubble plume, and the second is that of the flow structure of bubble for the different sections of bubble regions. The surface flow is effectively generated in case of bubble plume compared to liquid jet flow since the distortion point appears in the vicinity of surface. The flow structure and bubble parameters are sensitively modulated by the gas flow rate and bubble size.

Key words: Multiphase Flow, Bubble Plume, Surface Flow, Flow Visualization, Particle Imaging Velocimetry (PIV), Bubble

Introduction

In many engineering fields such as materials, chemical, mechanical, and environmental engineering, the techniques of gas injection have been widely utilized for improving chemical reactions, waste treatment, gas mixing and resolution, heat and mass transfer, and other engineering process.

Bubbly two-phase flows have various flow structures, which are not observed in a single-phase flow, due to the complexity of the translational motion and the volumetric change of the bubbles. The variety of the flow structure often considerably impacts the performance of hydraulic machinery and chemical and bioreactor in which the bubbly media is used as a working fluid. In particular, the local flow behavior such as the mutual interaction between bubbles and vortices influences the statistical characteristics of the flow. For instance, both the generation and deformation of vortices in the liquid phase due to the inhomogeneous buoyancy caused by the local distribution of

bubbles, and the accumulation of bubbles in the vortex cores and turbulence generation due to the bubble migration, enhance the flow instability and the turbulence modification. The bubble plume is a suitable object to analyze the detailed flow structure in bubble flow because it involves various interactions between the bubble and the ambient liquid flow when the bubble rises from the bottom to the upper free surface (Hassan 2002, 2003, 2006, 2011, Hassan and Tamer 2006, Murai and Matsumoto 1998, Matsumoto and Prosperetti 1997, Matsumoto and Murai 1995, Hassan et. all. 2001).

On the other hand, the behavior of bubbles in a liquid is fundamentally different from that of solid particles in a gas. Bubbles have essentially no mass compared to the surrounding liquid, but particle inertia dominates the surrounding gas. Therefore, bubble motion leads the fluid while particles lag and the relative velocity is generally positive for bubbles but negative for particles. In fact, there is an interaction between the bubble plume and its environment. Hence, measurements of the environment can be used to derive the entrainment flux to the plume. However, it is required to develop an expression for the relative velocity in order to study the response of bubbles to the surrounding liquid (Hassan 2003, 2006, 2011, Hassan and Tamer 2006, Stewart and Crowe 1992).

Flows including bubbles called “bubbly flow” frequently show a very complicated behavior due to a strong interaction between bubble and vortex motions, and such phenomena significantly govern the performance of various industrial and environmental systems and processes in which bubbles are used. These processes require to be improved further since their performances are strongly swayed by the characteristics of the bubble motion. In this case, we have, not only to grasp the rough flow pattern of the two phases formed by bubble injection or boiling, but also to quantitatively recognize the flow field in order to maintain or improve the performance of the system. If we could predict or accurately measure the detailed flow structure, we would be able to significantly improve the efficiency, stability, and controllability of the devices by using the obtained data.

Bubble plumes are observed in various engineering disciplines, e.g. in industrial, material, chemical, mechanical, civil, and environmental applications such as chemical plants, nuclear power plants, naval engineering, the accumulation of surface slag in metal refining processes, the reduction of surfactants in chemical reactive processes, chemical reactions, waste treatment, gas mixing and resolution, heat and mass transfer, aeronautical and astronautical systems, biochemical reactors as well as distillation plants, etc (Hassan 2002, 2003, 2006, 2011, Hassan and Tamer 2006, Hassan, et. al. 2001, Murai et. al. 2001, Abdel Aal et. al. 1966, Goosens and Smith 1975, Al Tawell and Landau 1977, Chesters et. al. 1980, Bankovic et. al. 1984, Sun and Faeth 1986, Szekely et. al. 1988, Gross and Kuhlman 1992, Bulson 1968).

Flows induced by a bubble plume are utilized in many industrial processes. The main features of this kind of flow are:

(1) A large scale circulation of the liquid phase can be generated in natural circulation systems like lakes, agitation tanks, etc.

(2) Strong rising flows can be induced by the pumping effect as in air-lifting pumps.

(3) High speed surface flows may be developed at the free surface, by which the density and the transportation of the surface floating substances can be controlled.

(4) High turbulence energies can be produced in the two-phase region due to the strong local interaction between individual bubbles and the surrounding liquid flow (Hassan 2002, 2003, 2006, 2011, Hassan and Tamer 2006, Murai et. al. 2001).

Surface flows generated by bubble plumes are considered as a key phenomenon in many processes in bioreactors, chemical plants, modern industrial technologies, such as metal refinement, and future-type nuclear power plants, in addition to the many applications of bubble plumes mentioned above. These processes, which are expected to be improved by applying the bubble plume, require the control of both concentration and transportation of surface-floating substances, i.e. solidized materials or impurities, as well as the stabilization of the interface motion itself in order to guarantee their designed performances. Hence, the flow in the vicinity of a free surface induced by a bubble plume was utilized as an effective way to control surface floating substances on lakes, rivers, seas, oceans, as well as in various kinds of reactors and industrial processes handling a free surface (Hassan 2002, 2003, 2006, 2011, Hassan and Tamer 2006, Hassan, et. al. 2001, Sheng and Irons 1992, Iguchi et. al. 1991, Tomiyama et. al. 1994).

The main reason for surface flows induced by bubble plumes to be utilized in so many fields

mentioned above is the simplicity of installation. However, from the fluid mechanical point of view, it is important to focus on the advantages of the bubble plume comparing to various other types of jet flows. As an example, Fig. 1 shows schematic figures of three types of the jet flows:

1) Single-phase liquid jet flow (water jet flow).
2) Single-phase buoyant jet flow.
3) Bubble plume induced flow.

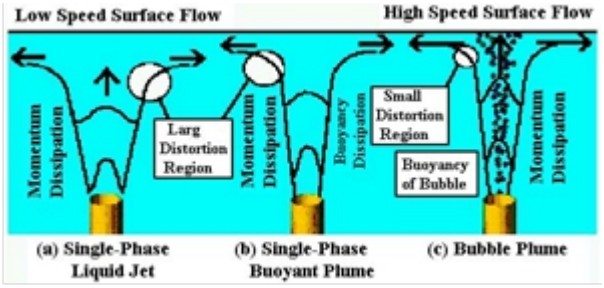

Fig. 1 Different surface flow generation mechanisms

1) In the case of the single-phase liquid jet flow (water jet flow), the maximum velocity in the jet decreases monotonically due to turbulent momentum diffusion, so that the width of the jet expands near the surface. The resultant thick layer surface flow will have a slow velocity.

2) In the case of a single-phase buoyant jet flow, the maximum velocity peak is flattened by the buoyancy effect. However, the buoyancy is dissipated due to turbulent mixing near the free surface so that no thin high speed surface flow occurs.

3) On the contrary, the bubble plume induced flow keeps its initial buoyancy even close to the surface since bubbles do not diffuse immediately (it is called immiscible buoyant jet). Furthermore, an individual bubble has motion characteristics different from surrounding liquid; therefore, the buoyancy distribution does not simply diffuse. The resultant surface flow is thinner and faster than in the first two cases. Hence, the surface flow is rather effective in case of the bubble plume compared to the first two flows because the distortion point occurs near the surface (Hassan 2002, 2003, 2006, 2011, Hassan and Tamer 2006, Hassan, et. al. 2001, Murai et. al. 2001).

Many researchers have carried out extensive model experiments by focusing on the flow field using air bubbles as gas injection through a bottom nozzle. This model is the most popular and has wide applications. Since bubble plumes have been used with varying degrees of success more information on the mentioned above subjects should be accumulated because there is still possible improvement to get higher efficiency for generating the surface flow (Hassan et. al. 2001, Gross, et. al. 1992, Sun, et. al. 1986, Hussain and Narang 1984, Hara, et. al. 1984, Chesters, et. al. 1980, McDougall 1978, Abdel-Aal, et. al. 1966, Hussain and Siegel 1976, Leitch and Baines 1989, Murai and Matsumoto 1998, Taylor 1955, Jones 1972, Murai, et. al. 2001).

This paper is concerned with the characteristics of bubble induce the surface flow (the detailed structure of surface flow generation mechanism), which depends on the gas flow rate, the bubble size, and the internal two-phase flow structure of the bubble plume. Particle Imaging Velocimetry (PIV) including Particle Tracking Velocimetry (PTV) and numerical simulation model using (E-L model) (Murai and Matsumoto 1996 and 1999) are applied after carrying out two kinds of flow visualization in order to evaluate their parameter relationships. The first one is visualization of the whole field around the bubble plume, and the second that of the different sections of bubble regions in order to clarify the relationship between bubble parameters (gas volume flow rate, mean bubble diameters and void friction). It is confirmed by this paper that the experimental results resemble the numerical results. The relationship between the maximum surface flow velocity and the bubble generation condition in the surface flow generation process is explained.

Experimental Apparatus, Method and Conditions:

Experimental apparatus for carrying out the experiments of bubble parameters and the flow pattern around a bubble plume (whole field flow structure) is constructed as shown in figure 2. The inner tank size is 1300 mm in length, 1000 mm in height, and 110 mm wide, made of transparent acrylic resin. The experimental and simulation conditions are listed up in Table 1.

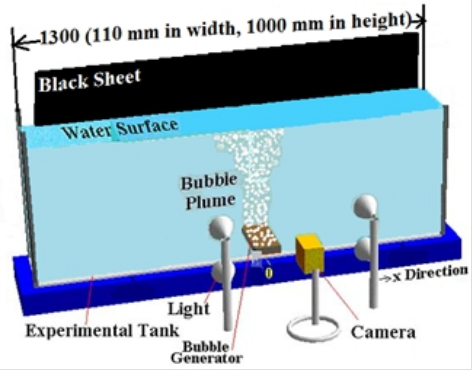

Fig. 2 Schematic diagram of experimental setup

Table 1: Experimental and simulation conditions

Parameter	Value
Density of water	ρ=1000 kg/m^3
Kinematic viscosity of water	υ =10^{-6} m^2/s
Initial water height	H =0.2 ~ 0.6 m
Atmospheric pressure	101 kPa
Temperature of environment	22-25 °C
Density of gas (air)	1.25 kg/m^3
Maximum gas flow rate	8.0 × 10^{-6} m^3/s

The bubble generator is installed at the center of the bottom part of the tank. Four kinds of bubble generators (with different injector nozzles) are applied for the experiments. Table 2 shows the experimental conditions for bubble generators. The gas flow rate is precisely controlled by a pressure regulator and a flowmeter. A lighting setup (direct lightning method) with a black back sheet background and two halogen lamps of 1000 W is used to clearly visualize and take the images of the experiments and for the PIV measurements. The visualized flows are recorded by a digital video camera (Panasonic DMC-GH2H) that captures 30 fps. The digital images are preprocessed through the video to JPEG converter image software and Adobe After Effects CS6 image processing software. The preprocessing entails sharpening, binarizing and smoothing of the images, and labeling bubbles and particles.

Table 2: Experimental conditions for bubble generators

	Bubble Generator-	Bubble Generator-	Bubble Generator-3	Bubble Generator-4
Type	Block	Straight	Round Shape	Single Nozzle
Number of Nozzles	14	16	39	1
Nozzle Diameter	0.75 mm	1 mm	1 mm	5 mm
A (mm^2) Injector	65×20	120×1	150×45	19.63
Air Tube/ Room	80×55×25	6.5 mm	6.5 mm	6.5 mm

Bubble Parameters Calculations:

Table 3 shows the calculations of mean (average) bubble diameter for the four types of bubble generators and for water height of 200, 400 and 600 mm respectively and for six ranges of gas volume flow rates [Qg_{-1} to Qg_{-6}]. Therefore, seventy two cases (conditions) are handled in these experiments. The values in this table are calculated by using the time average of 180 consecutive frames in the image processing (6 seconds). The averaged bubble diameter, the void fraction, the width of bubble injection and the standard deviation are calculated by measuring more than 1200 bubbles in the local VTR images inside the bubble plume using image processing. These images are taken by recording local pictures of different regions; the injector region of the bubble generator, the middle reigns and near the free surface. Figure 3 shows samples of bubble images for different condition of bubble generators. The bubble diameter is defined by the equivalent bubble diameter using ellipsoidal approximations for the bubble shapes. The equivalent bubble diameter is estimated by the vertical and

the horizontal lengths of each bubble of the image object, which are obtained by using the JPEG converter image software and Adobe After Effects CS6 image processing software after binarizing the images. The measurement uncertainty (standard deviation) for the bubble diameter is estimated to be around (0.01~0.015 mm) of the averaged bubble diameter according to the pixel resolution. This reflects the accuracy of the experimental results.

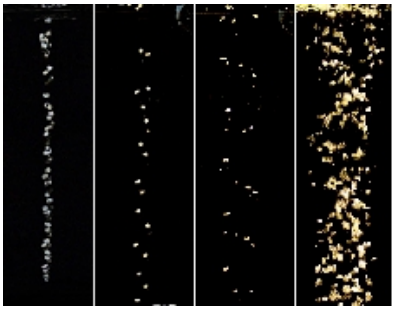

Fig. 3 Samples of Bubble Images for Different Condition of Bubble Generators

Table 3: Mean bubble diameter for water height H=200, H=400 and H=600 mm

Gas volume flow rate Q_g [m^3/s]	**Mean bubble diameter D (mm) for water height H=200, 400, 600 mm**											
	Bubble Generator-1			**Bubble Generator-2**			**Bubble Generator-3**			**Bubble Generator-4**		
	H=	**H=**	**H=**	**H=**	**H=**	**H=**	**H=**	**H=**	**H=**	**H=**	**H=**	**H=**
$Q_{g1}=0.56\times10^{-6}$	2.8	6.01	6.87	3.0	6.89	7.80	3.80	7.00	8.90	6.20	8.10	9.54
$Q_{g2}=1.11\times10^{-6}$	3.0	6.30	7.54	3.4	7.17	8.10	4.02	7.55	9.20	6.70	8.70	9.91
$Q_{g3}=1.67\times10^{-6}$	3.3	6.70	8.06	3.6	7.84	8.90	4.95	8.25	9.80	6.95	9.60	10.3
$Q_{g4}=2.22\times10^{-6}$	3.6	7.15	8.41	3.9	8.09	9.20	5.90	8.55	10.1	7.40	10.01	10.7
$Q_{g5}=3.33\times10^{-6}$	4.0	7.60	9.01	4.1	8.72	9.50	6.80	8.95	10.6	7.90	10.80	11.2
$Q_{g6}=7.00\times10^{-6}$	6.5	10.80	12.30	7.1	11.80	13.5	9.12	12.70	15.6	10.80	15.89	17.8

Figure 4 shows the relationship between the mean (average) bubble diameter and the gas volume flow rates for the four types of bubble generators for water height of 200, 400 and 600 mm respectively. These figures confirm that as the gas volume flow rates increases the mean (average) bubble diameter increases.

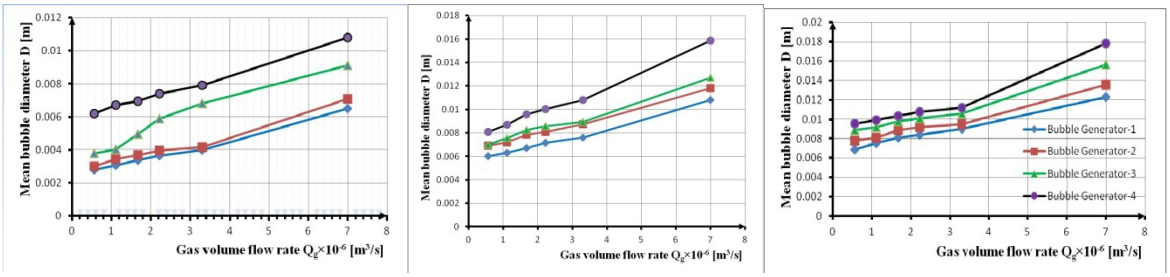

Fig. 4 The relationship between gas volume flow rate and mean bubble diameter for H=200, H=400 and H=600 mm respectively

On the other hand, the void fraction (α) is calculated by using the equation ($\alpha=Q_g/A\times V_b$) (Hassan et. al. 2001, Hassan 2002, 2003, 2006, 2012, Isao et. al 1993, Murai et. al. 1998, 2001 and Matsumoto et. al. 1995-B), where A is the area of calculation in the injector region, (injector surface of the bubble generator) as shown in table 4. The bubble rising velocity V_b is about 0.20 to 0.30 m/s. The bubble rise velocity is unsteady at the beginning (at the nozzle exit) and after a short period of time it reaches the terminal rise velocity. The measurement uncertainty for the rising bubble velocity is estimated to be about 2%. The relative velocity between the bubbles and the liquid flow corresponds well to the terminal rising velocity of the bubble in a quiescent liquid.

Table 4: Void fraction for bubble generator type

Gas volume flow rate Q_g [m^3/s]	Void fraction α			
	Bubble Generator-1	Bubble Generator-2	Bubble Generator-3	Bubble Generator-4
$Q_{g1}=0.56\times10^{-6}$	0.0022	0.0009	0.0004	0.1425
$Q_{g2}=1.11\times10^{-6}$	0.0039	0.0017	0.0007	0.2567
$Q_{g3}=1.67\times10^{-6}$	0.0053	0.0023	0.0010	0.3539
$Q_{g4}=2.22\times10^{-6}$	0.0065	0.0028	0.0012	0.4350
$Q_{g5}=3.33\times10^{-6}$	0.0091	0.0039	0.0018	0.6050
$Q_{g6}=7.00\times10^{-6}$	0.0179	0.0078	0.0035	1.1881

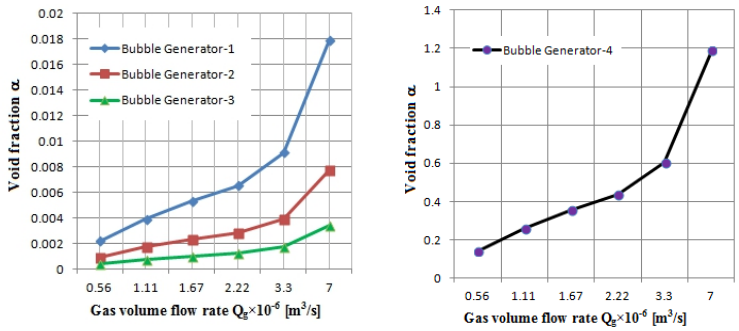

Fig. 5 The relationship between gas volume flow rate and void fraction α

Figure 5 shows the relationship between the void friction of the four types of bubble generators and the gas volume flow rates. These figures confirm that as the gas volume flow rates increases the void friction increases. Moreover, the void friction increases with the gas flow rate at a power index of around 0.8 to 1.0 [$\alpha\ \alpha\ Qg^{(0.8\sim1.0)}$]. The measurement uncertainty for the void fraction is estimated to be about 2 to 3%.

Figures 6 and 7 show the relationship between mean bubble diameter and water height in the tank for the four bubble generator types and for the six gas volume flow rate. It is clear from these figures that the bubble size increases as the water height in the tank increase.

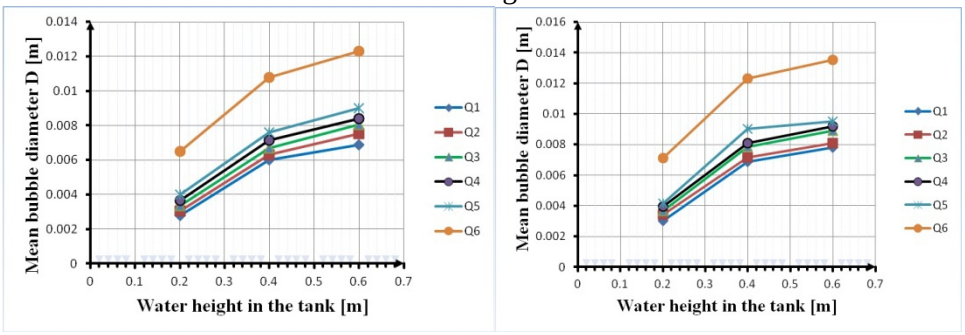

Fig. 6 The relationship between mean bubble diameter and water height in the tank for bubble generator -1 and bubble generator -2 and for the six gas volume flow rate

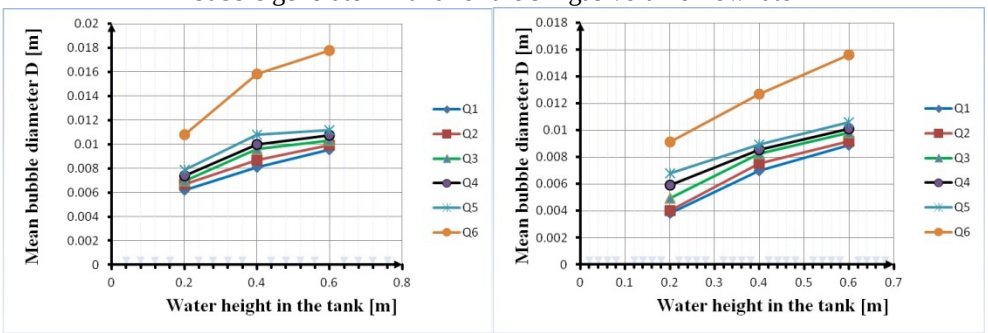

Fig. 7 The relationship between mean bubble diameter and water height in the tank for bubble generator -3 and bubble generator -4 and for the six gas volume flow rate

Flow Pattern around a Bubble Plume (Whole Field Flow Structure):

In order to clarify the flow pattern of the internal liquid flow (the whole field flow structure around the bubble plume) in water tank, spherical particles made of a high-porous polymer with diameters of 200 to 600 μm and a density of 1010 kg/m^3, are seeded in the entire tank as tracer particles for the PIV measurement and then the flow is visualized. The recorded images are ported to a computer. The flows are measured in this section by using the PIV technique measurements for [case-1]: bubble generator-2 and gas flow rate value of $Q_{g5}=3.33\times10^{-6}$, [case-2]: bubble generator -1 $Q_{g6}=7.00\times10^{-6}$.The height of water (H) in the tank is 600 mm.

Fig. 8 shows a sample the recorded image of the seeded flow field around a bubble plume for the case-1 and case-2. In these images the bubble plume is located in the middle of the images, while the particles are distributed around the bubble plume. After these images are ported to a computer, velocity vector maps are obtained by using the BDCC (Brightness Distribution Cross-Correlation) method (Adrian et. al. 1991 and Kimura et. al. 1986) as shown in Fig. 9.

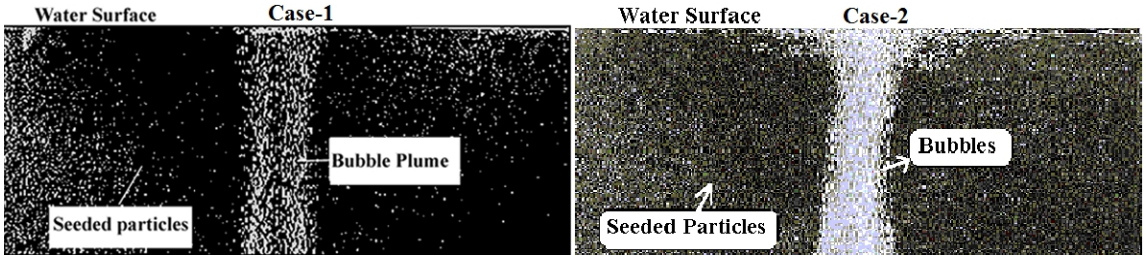

Fig. 8 Seeded image for PIV measurements (the image of the global motion) for [case-1] and [case-2]

It is follows from these figures that the resulting flow is steady and symmetric relative to the bubble plume center (especially when a small gas flow rate is given). The flow pattern depends on the gas flow rate, and as the gas flow rate increases, the magnitude of velocity (the mean velocities of liquid phase and gas phase) increases and the effective area of the bubble plume (of the surface flow) expands in horizontal direction. The detailed flow mechanism can be explained as follows. The main upward liquid flow is driven along the bubble plume by the rising bubbles. Then the main flow reaches up to the free surface. The momentum of the upward flow becomes maximum near the liquid surface. Just under the free surface the upward flow rapidly changes its orientation into a horizontal flow. Then, a pair of liquid circulations is generated beside the bubble plume. By this symmetrical circulation, the main vertical flow is sharply converted to a strong surface flow. After same time, the pair of liquid circulations induces a whole scale circulation of the liquid over the entire tank. Also, since it induces an entrainment flow at the bottom region, total flow rate of main flow increases and more effective surface flow is generated.

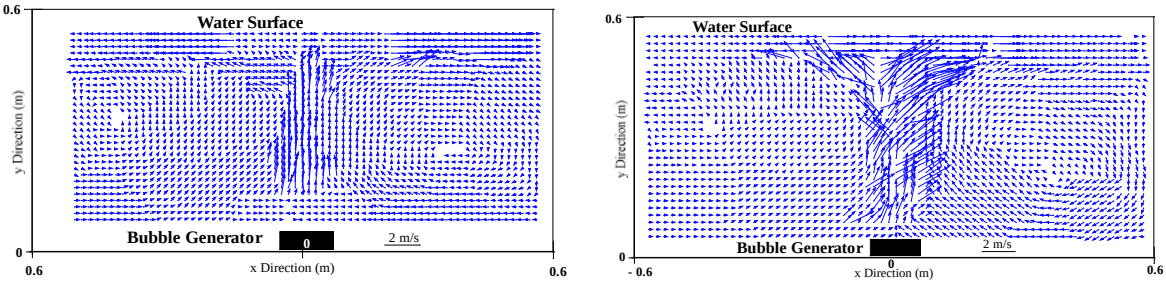

Fig. 9 Velocity vector map for [case-1] and [case-2]

The numerically simulation predicted results (which are done for comparing their results with PIV results) are obtained by solving seven governing equations (Matsumoto and Murai 1995, Murai and Matsumoto 1996, Hassan 2003, 2007). These calculations are for [case-1]. The simulation period for numerical predictions is about 0 to 120 seconds. The numerically predicted results shown in Fig. 10 indicates a time-development of whole-field flow structure (liquid velocity vector and bubble distributions) generated by the bubble plume. Although at the initial stage (T<2) only a vertical liquid flow is induced along the bubble plume, the flow region expands widely and a strong surface flow is

stably maintained and well-developed stage. Also, the predicted local flow near the bubble plume is in good agreement with the PIV measured velocity map.

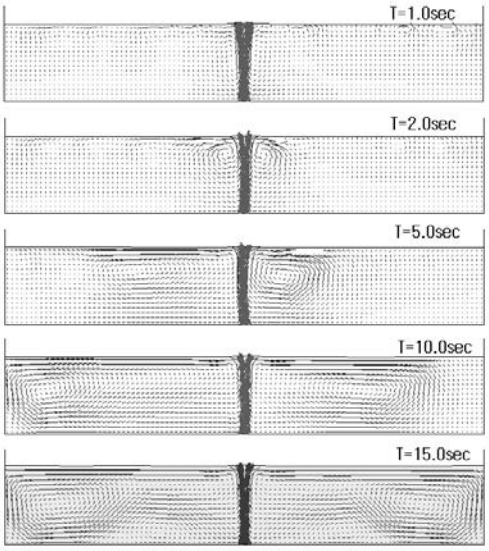

Fig. 10 Global field flow structure (liquid velocity vector and bubble distribution) for [case-1]

Fig. 11 shows samples of the whole field structure instantaneous streamlines during periodic swaying motion of the bubble plume (for the same cases "case-1 and case–2"), which are calculated by time-integrating of the measured velocity vector maps after calculating the stream function. The following two matters can clearly be recognized in these figures.

(1) The main upward flow converges and accelerates along the bubble plume. This phenomenon is completely different from a single-phase jet structure.

(2) The flow near the liquid surface is much larger than that in other regions.

Table 5 presents the relationship between gas flow rate and the width area of the bubble plume on the surface (the area which contains bubbles on the free surface "the width of the surface flow" in the horizontal direction), which is measured from video images. It is confirmed by this table that this area increases approximately proportional to the square root of the gas flow rate.

Table 5: The relationship between gas flow rate and area width of the bubble plume on the free surface

Gas flow rate (m^3/s)	Area width (m)
$Qg = 2.22\times10^{-6}$	0.225
$Qg = 3.33\times10^{-6}$	0.415
$Qg = 7.00\times10^{-6}$	0.530

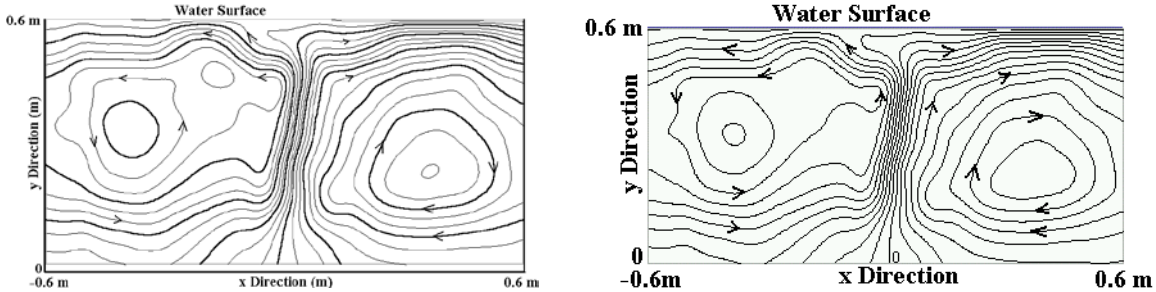

Fig. 11 Streamlines obtained by PIV for [case-1] and [case-2]

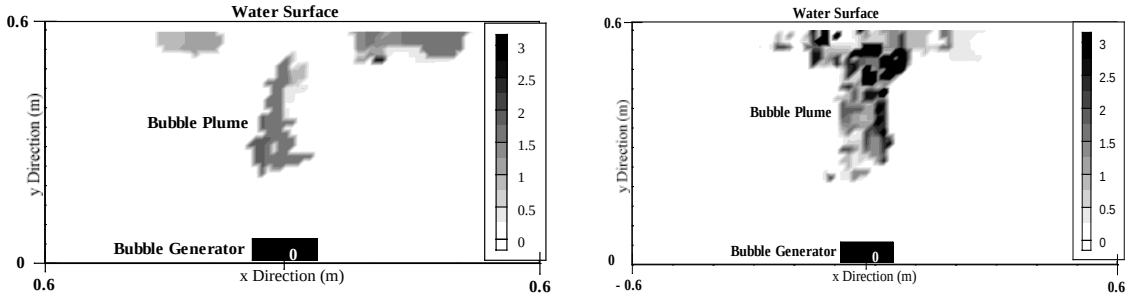

Fig. 12 Kinetic energy distribution $(m/s)^2$ for [case-1] and [case-2]

Moreover, in order to clarify the detailed structure of the flow, the two-dimensional distribution components of the specific kinetic energy and the vorticity are calculated. These values are calculated from the measured velocity vector map, where the velocity inside the bubble plume contains two different phases, a liquid phase and a gas phase. Fig. 12 shows the kinetic energy distribution for the same cases "case-1 and case–2", while Fig. 13 shows the vorticity distribution for the same cases.

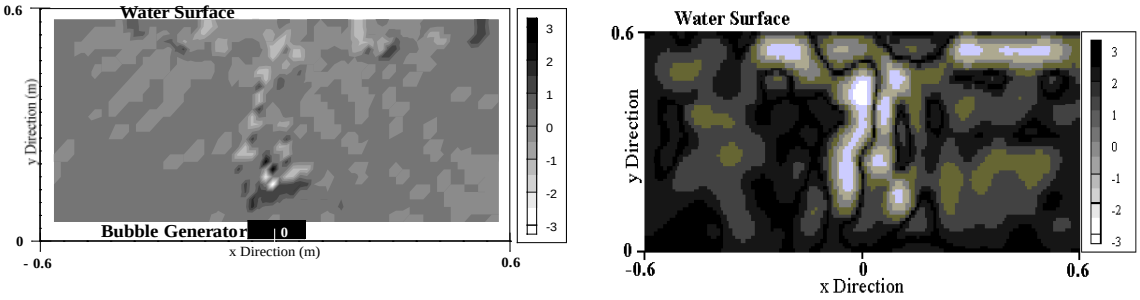

Fig. 13 Vorticity distribution (s^{-1}) for [case-1] and [case-2]

It is clear that the highest kinetic energy is generated far up (in the center of) the bubble plume and in the vicinity of the free surface. This observation confirms the idea that the bubble plume can generate a strong and wide surface flow over the bubble generation system. Beyond that, the figures of the vorticity distribution show that the rapid distortion or the rotation flow occurs in the area under the free surface where the upward flow changes its orientation from vertical into horizontal direction.

As our future works, the similarity between laboratory model and an actual application scale should be analyzed as well as three-dimensional interferences. Moreover, the relationship between mean bubble diameter and water height in the tank should be addressed for larger range of water height in the tank in order to find the ideal parameters for real application.

Conclusion

As a result, it is clear that the bubble plume "which is a typical bubble flow" is a key phenomenon to be studied and investigated, and it is an effective tool for many applications and can indeed contribute to various improvements. The motivation to study the bubble plume is the demands to improve its performance and its applications. Especially in many engineering fields as materials, chemical, mechanical, modern industrial technologies, and in the environment in order to protect the natural environment, the naval planets, navel systems, rivers, lakes, etc from pollution. Hence these engineering fields are expected to benefit from the improvement and development of the bubble plume.

Flow in the vicinity of a free surface, which is induced by a bubble plume is utilized as an effective way to control surface floating substances on lakes and oceans, as well as in various kinds of processing and industries handling free surfaces.

Surface flows are more effectively generated by bubble plumes compared to liquid jet flows because the distortion point appears in the vicinity of the surface.

Flow visualization, image analysis using PIV and numerical simulation of the bubble plume are carried out in order to improve the applicability of the bubble plume. The flow pattern for the whole field flow structure of the bubble plume is demonstrated. The parameters of bubbles are

calculated. The experimental results and the numerical results show good analogy. The flow structure is sensitively modulated by the gas flow rate and bubble size, and the main results can be summarized as follows:

1) There are two large circulation flow regions of liquid near the bubble plume (at the right and the left side of the bubble plume).

2) The local liquid flow pattern around the bubble plume depends on the gas flow rate. It is recognized that as the gas flow rate increases, the magnitude of velocity increases and the effective area of the bubble plume (the width of the surface flow) expands in the horizontal direction.

3) Inside the bubble plume and near the free surface, the velocity of the two-phase flow is higher while it is slower in other regions. Hence, high speed two-phase flow is maintained and further accelerated along the vertical axis, and it produces large entrainment flow in the lower region. This is due to the effect of the buoyancy of bubbles. Hence, the generation of this high speed flow is considered a main contribution to induce a strong surface flow. If a vertically rising liquid jet is applied to induce the surface flow instead of the bubble plume, the high speed upward flow is not maintained near the free surface due to the turbulent momentum dissipation and the lack of the buoyancy inside the jet, and in this case the power efficiency is considerably less due to the dissipation of momentum under the free surface.

4) The spacing of the streamlines becomes smallest at the free surface. Moreover, near the free surface, the liquid flow in the horizontal direction is maintained over long distances. Hence, the maximum velocity in the horizontal direction is observed to be near the free surface. This means that the horizontal velocity is fastest on the free surface since there is no shear stress acting on the free surface. This is also one of the reasons why such a wide and thin surface flow is generated by the bubble plume.

5) The highest kinetic energy is generated at a long distance (far up) inside the bubble plume and in the vicinity of the free surface. This observation confirms the fact that the bubble plume can indeed generate a strong and wide surface flow over the bubble generation system.

6) High vorticity distribution is generated by the surface flow, which induced by the bubble plume, and these phenomena appear in a layer under the free surface. In this layer the liquid flow rapidly changes its orientation from the vertical to the horizontal direction. Therefore, it can be said that the initial surface flow is rapidly generated in this layer. Therefore, the rapid distortion of the liquid phase results just under the free surface. This is qualitatively different from (not found so clearly in) the case of a single-phase liquid jet flow whose speed is equivalent to the bubble plume. These results indicate that a surface flow is more effectively generated by means of bubbles than by a liquid jet flow because the distortion point appears in the vicinity of surface.

References:

Abdel-Aal H. K., Stiles G. B. and Holland C. D. 1966. Formation of Interfacial Area at High Rates Gas Flow Through Submerged Orifices. ALCHE J. 12, pp. 174-180.

Adrian, R. J. 1991. Particle-Imaging Techniques for Experimental Fluid Mechanics. Annu. Rev. Fluid Mech. Vol. 23. Pp. 261-304.

Al Tawell A. M. and Landau J. 1977. Turbulence Modulation in Two-Phase Jets. Int. J. Multiphase Flow 3, pp. 341-353.

Bankovic A., Currie, I. G. and Martin W. W. 1984. Laser-Doppler Measurements of Bubble Plumes. Phys. Fluids 27, pp. 348-355.

Bulson P.S. 1968. The Theory and Design of Bubble Breakwaters. Proc. 11th Conf. Coastal Engng, London. 995.

Chesters A. K., Van Doorn M. and Goossens L. H. J. 1980. A General Model of Unconfined Bubble Plumes from an Extended Source. Int. J. Multiphase Flow 6, pp. 499-521.

C. W. Stewart and C. T. Crowe 1992. Bubble Dispersion in Free Shear Flows. Int. J. Multiphase Flow Vol. 19. No. 3, pp. 501-507. 1992. Great Britain.

Goosens L. H. J. and Smith J. M. 1975. The Hydrodynamics of Unconfined Bubble Columns for Mixing Lakes and Reservoirs. Chem. Eng. Tech. 47, 951. PP. 249-261.

Gross R. W. and kuhlman J. M. 1992. Three-Component Velocity Measurements in a Turbulent Recarculating Bubble-Driven Liquid Flow. Int. J. Multiphase Flow 18, 413-421.

Hara, S., Ikai, M., Namie, S. 1984. Fundamental Study on an Air Bubble Type of Oil Boom. Trans. Ship-Making Society of Kansai-Japan. Vol. 194.
Hassan Abdulmouti, Yuichi Murai, Yasushi Ohno and Fujio Yamamoto 2001. Measurement of Bubble Plume Generated Surface Flow Using PIV. Journal of the Visualization Society of Japan. Vol. 21. No. 2. Pp. 31-37
Hassan Abdulmouti 2002. The Flow Patterns in Two Immiscible Stratified Liquids Induced by Bubble Plume. The International Journal of Fluid Dynamic. Vol. 6. Article 1.
Hassan Abdulmouti 2003. Visualization and Image Measurement of Flow Structures Induced by a Bubbly Plume. Ph. D. thesis. Fukui University.
Hassan Abdulmouti. Bubbling Convection Patterns in Immiscible Two-phase Stratified Liquids. International Journal of Heat Exchangers (IJHEX). Vol. VII. No. 1. Pp. 123-143. ISSN 1524-5608. June 2006.
Hassan Abdulmouti and Tamer Mohamed Mansour. Bubbly Two-Phase Flow and Its Application. 10th International Congress on Liquid Atomization and Spray Systems (ICLASS-2006). Aug. 27-Sept. 1. Kyoto, Japan. 2006.
Hassan Abdulmouti. Surface Flow Generation Mechanism Induced by Bubble Plume. Yanbu Journal of Engineering and Science (YJES). Second issue. PS-M02-28 (50-67). 2011.
Hussain N. A. and Siegel R. 1976. Liquid Jet Pumped by Rising Gas Bubbles, J. Fluids Eng., March 8. Pp. 49-62.
Hussain N. A. and Narang B. S. 1984. Simplified Analysis of Air-Bubble Plumes in Moderately Stratified Environments. ASME. Journal of Heat Transfer. Vol. 106, pp. 543-551.
Iguchi M., Takehuchi H. and Morita Z. The Flow Field in Air-Water Vertical Bubbling Jets in a Cylindrical Vessel, ISIJ International J., 31, 3. 1991, 246-253.
Isao Kataoka, Akimi Serizawa and D. C. Besnard. 1993. Prediction of Turbulence Suppression and Turbulence Modeling in Bubbly Two-Phase Flow. Nuclear Engineering and Design 141. 1993. 145-158. North-Holland.
Jones W. T. 1972. Air Barriers as Oil-Spill Containment Devices. J. Soc. Pet. Engng.. Pp.126-142.
Kimura, I., Kimura, H., Takamori, T. 1986. Image Processing of Flow around a Circular Cylinder by Using Correlation Techniques. Proc. 4th Int. Int. Symp. Flow Visualization, Hemisphere. Pp. 221-226.
Leitch, A. M., and Baines, W. D. 1989. Liquid Volume Flux in a Weak Bubble Plume, J. Fluid Mech., 205. Pp. 77-98.
Matsumoto Y., Murai Y.. (1995). The Numerical Simulation of Bubble Plume in Container Have Free Surface. Trans. JSME B, 61-588. 2818-2825.
Matsumoto Y. and Murai Y. 1995. Trans. Jpn. Soc. Mech. Eng., Vol.61, No. 588, B 1995, pp.2818-2825.
Matsumoto, Y., Murai, Y. 1995-B. Numerical Simulation of Bubble Plume in a Tank with Free Surface. Trans. Jpn. Soc. Mech. Eng.. Vol. 61. No. 588. B. Pp (54-61).
Matsumoto Y. and Prosperetti A. 1997. Edit., Proc. ISAC'97 High Performance Computing on Multi-phase Flows.
McDougall T. J. 1978. Bubble Plumes In Stratified Environments. Journal of Fluid Mechanics, Vol. 85, 1978, pp. 655-672.
Murai Yuichi, Ido Takehiro, Ishikawa Masa-aki Yamamoto Fujio. (1998). Development of the Post-Processing Method for PIV Measurement Result Using Computational Fluid Dynamics Procedure. Transaction of the Japan Society of Mechanical Engineers 64B-626. Pp.109-116.
Murai Y., Matsumoto Y., Sou K., Yamamoto F.. (1998). The Numerical Simulation of Disorder Structure Formed by Bubbly Buoyant Force. Trans. JSME B, 64-626. 3257-3262.
Murai Yuichi, Ohno Yasushi, Abdulmouti Hassan, Yamamoto Fujio 2001. Flow in the Vicinity of Free Surface Induced By a Bubble Plume. JSME. 067, 657, B.
Murai Y. and Matsumoto Y. 1996. Numerical Simulation of Turbulent Bubble Plumes Using Eulerian- Lagrangian Bubbly Flow Model Equation. Proc. Int. Symp. on Mathematical Modeling of Turbulent Flows pp. 233-238.
Murai Y. and Matsumoto Y. 1998. Numerical Analysis of Detailed Flow Structures of a Bubble Plume. JSME International Journal, Series B, Vol. 41, No. 3, 1998. Pp.568-575.

Murai, Y., Matsumoto, Y. 1999. Eulerian Analysis of Bubbly Two-Phase Flows Using CIP Scheme. Computational Fluid Dynamics Journal. Vol. 8 No. 1 April.
Sheng, Y.Y., and Irons, G.A.: Measurements of the Internal Structure of Gas-Liquid Plumes, Metallurgical Trans., Vol. 23-B. 1992, 779-788.
Sun T. Y. and Faeth G. M. 1986 a. Structure of Turbulent Bubbly Jets-I. Methods and Centerline properties. Int. J. Multiphase Flow 12, pp. 99-114.
Szekely, J., Carlson, G. and Helle L. 1988. Ladel Metallurgy. Springer. Berlin.
Taylor Sir Geofffery. The action of a Surface Current Used as a Breakwater, Proc. Royal Society, A., Vol. 231, 1955, p. 466-478.
Tomiyama, A., Uegomori,S., Minagawa,H., Fukuda,T. and Sakaguchi,T. Numerical Analysis of Bubble-Induced Natural Circulation based on Multidimensional Two-Fluid Model, Trans. JSME (Jpn. Soc. Mech. Eng.), 60-580, B, 1994, 9-14.